PHYSICAL REVIEW B VOLUME 59, NUMBER 2 1 JANUARY 1999-II

Characterization of a quasi-one-dimensional spin-1/2 magnet which is gapless and paramagnetic for $g\mu_B H \lesssim J$ and $k_B T \ll J$

P. R. Hammar, M. B. Stone, and Daniel H. Reich
Department of Physics and Astronomy, The Johns Hopkins University, Baltimore, Maryland 21218

C. Broholm
Department of Physics and Astronomy, The Johns Hopkins University, Baltimore, Maryland 21218
and NIST Center for Neutron Research, National Institute of Standards and Technology, Gaithersburg, Maryland 20899

P. J. Gibson, M. M. Turnbull, and C. P. Landee
Carlson School of Chemistry and Department of Physics, Clark University, Worcester, Massachusetts 01610

M. Oshikawa
Department of Physics, Tokyo Institute of Technology, Oh-oka-yama, Meguro-ku, Tokyo 152-8551, Japan

(Received 27 August 1998)

High-field magnetization, field-dependent specific heat measurements, and zero-field inelastic magnetic neutron scattering have been used to explore the magnetic properties of copper pyrazine dinitrate $[\mathrm{Cu(C_4H_4N_2)(NO_3)_2}]$. The material is an ideal one-dimensional spin-1/2 Heisenberg antiferromagnet with nearest-neighbor exchange constant $J = 0.90(1)$ meV and chains extending along the orthorhombic a direction. As opposed to previously studied molecular-based spin-1/2 magnetic systems, copper pyrazine dinitrate remains gapless and paramagnetic for $g\mu_B H/J$ at least up to 1.4 and for $k_B T/J$ at least down to 0.03. This makes the material an excellent model system for exploring the $T = 0$ critical line that is expected in the H-T phase diagram of the one-dimensional spin-1/2 Heisenberg antiferromagnet. We present accurate measurements of the Sommerfeld constant of the spinon gas versus $g\mu_B H/J < 1.4$ that reveal a decrease of the average spinon velocity by 32% in that field range. The results are in excellent agreement with numerical calculations based on the Bethe ansatz with no adjustable parameters. [S0163-1829(99)11201-3]

I. INTRODUCTION

Quantum many-body systems that support qualitatively different ground states as a function of Hamiltonian parameters have the potential to display so-called quantum critical phenomena when these parameters are tuned in the vicinity of zero-temperature phase transitions.[1,2] Many unusual physical phenomena such as heavy-fermion behavior,[3] high-temperature superconductivity,[4,5] and non-Fermi-liquid behavior[6] are now thought to be manifestations of proximity to such quantum critical points. To understand the intrinsic properties of quantum criticality it is important to explore its phenomenology in simple and well-controlled model systems. One of the simplest quantum critical many-body systems is a linear chain of antiferromagnetically coupled spin-1/2 objects. Quantum criticality in this system is particularly interesting because it is possible to continuously tune the critical exponents by the application of a magnetic field.[7–9]

Unlike both conventional ordered magnets and gapped quantum spin chains that generally have sharp, low-energy dispersive modes, the excitation spectrum of the $S = 1/2$ antiferromagnetic (AFM) chain is dominated by the so-called ‘‘spinon continuum,’’[10,11] which is sketched in Fig. 1. Some properties of the $S = 1/2$ AFM chain may be computed exactly using the Bethe ansatz,[12] but it is also very illuminating to map the spin chain onto a one-dimensional system of interacting fermions.[13] This gives important insight into the spinon continuum, which may be viewed as the particle-hole continuum of the fermion model. This underlying fermion character of the $S = 1/2$ chain also has consequences for thermodynamic properties such as the magnetization and specific heat. There are a growing number of magnetic materials in which the predictions of these models have been tested experimentally.[14–18]

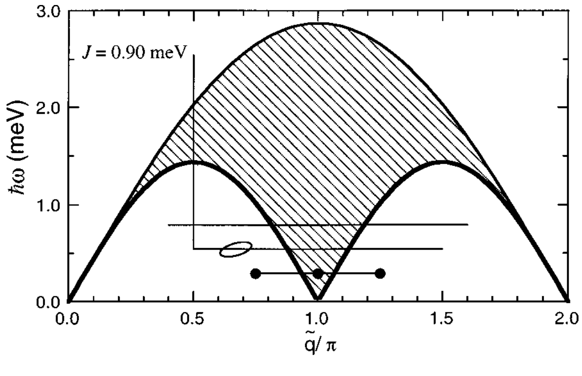

FIG. 1. Schematic view of the bounds of the spinon continuum of the $S = 1/2$ AFM chain, drawn for $J = 0.90$ meV as appropriate for CuPzN. Solid dots show fixed values of $\tilde{q}$ for the data in Fig. 6. Horizontal and vertical lines show the scan directions for the data in Figs. 7 and 8. The ellipse indicates the FWHM instrumental resolution for Figs. 7 and 8.

0163-1829/99/59(2)/1008(8)/$15.00

In the presence of a magnetic field H, an isotropic spin chain is described by the Hamiltonian

$$\mathcal{H}=\sum_{i}\,[J\mathbf{S}_i\cdot\mathbf{S}_{i+1}-g\mu_B\mathbf{H}\cdot\mathbf{S}_i]. \tag{1}$$

The field causes a Zeeman splitting of the half-filled, doubly degenerate spinon band, which introduces additional low-energy spanning vectors, and the spin chain has been predicted[11] to develop new soft modes at wave vectors that are incommensurate with the lattice, but which connect the field-dependent Fermi points. The dynamic critical exponents that control the temperature dependence of spin fluctuations close to these soft points are predicted to vary continuously with applied field. In a recent experiment on copper benzoate we have obtained the first direct experimental evidence for the existence of these low-energy modes.[18] However, while this work showed directly the field-induced incommensurability of the $S=1/2$ chain, it also showed a field-induced gap in copper benzoate. Oshikawa and Affleck showed[19] that this gap arises from the presence of two Cu sites per unit cell along the copper benzoate chains. The combination of a staggered g tensor and Dzyaloshinskii-Moriya interactions induces an effective staggered field when a uniform field is applied and this in turn creates a gap in the excitation spectrum and other interesting changes in the dynamic spin correlations.[19,20]

The result of this is that copper benzoate does not have a quantum critical line in the H-T plane because a field immediately drives the system away from criticality. In this paper we describe measurements on a long neglected one-dimensional spin-1/2 AFM, copper pyrazine dinitrate (CuPzN), which remains gapless for $g\mu_BH\lesssim J$ and $k_BT\ll J$, and thus is very well suited for experimental studies of quantum criticality. CuPzN is a $S=1/2$ chain with intrachain exchange constant $J\approx0.91$ meV $(J/k_B\approx10.6$ K), as determined from previous zero-field susceptibility and specific heat studies.[21,22] It is highly one-dimensional; three-dimensional ordering having not been observed in zero field for $T>0.1$ K,[22] which implies[23] that the ratio of interchain to intrachain coupling is $J'/J<10^{-4}$. The magnitude of the exchange constant J in CuPzN makes the material an attractive candidate for both thermodynamic and neutron-scattering studies in magnetic fields, as large effective fields $g\mu_BH/J$ can be obtained. We report high-field magnetization, field-dependent specific heat, and zero-field inelastic neutron-scattering measurements that show that CuPzN is a nearly ideal example of an isotropic Heisenberg AFM chain. In addition, our high-field specific heat data provide direct experimental evidence for the suppression with field of the spinon velocity in the one-dimensional spin-1/2 AFM.

II. COPPER PYRAZINE DINITRATE

CuPzN, $\mathrm{Cu(C_4H_4N_2)(NO_3)_2}$, is orthorhombic, with space group $Pmna$ and room-temperature lattice constants $a=6.712$ Å, $b=5.142$ Å, and $c=11.732$ Å.[24] The copper ions form chains along the [100] direction, with one copper per unit cell along the chain. The Cu ions along the chain are coupled magnetically through the pyrazine molecules, as shown in Fig. 2. The room-temperature g factors are $g_a=2.05$, $g_b=2.27$, and $g_c=2.07$.[25]

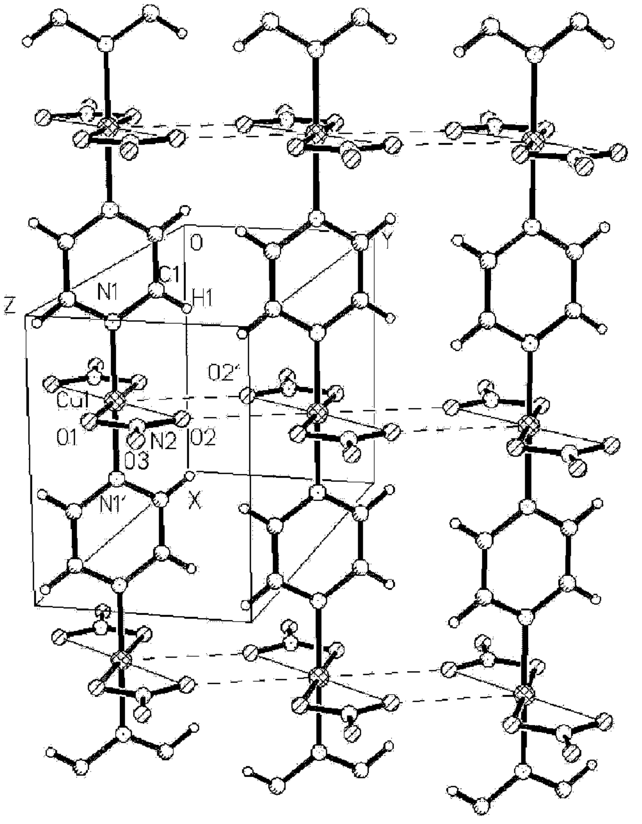

FIG. 2. Crystal structure of copper pyrazine dinitrate, $\mathrm{Cu(C_4H_4N_2)(NO_3)_2}$, showing how $\mathrm{Cu^{2+}}$ ions (hatched spheres) are linked through pyrazine rings to form one-dimensional chains. The chain axis (**a**) is vertical on the page, with the **b** axis nearly horizontal. The long bonds between the O2 atoms and the copper sites are represented by thin lines (intrachain contacts) and dashed lines (interchain contacts). Atomic positions are given in Table I, and bond lengths and angles are given in Table II.

We have redetermined the crystal structure of CuPzN with x rays at $T=158$ K.[26] There are no major differences from the room-temperature structure as originally determined. [24] The cell parameters show very slight contraction upon cooling along the chain axis a (6.712 Å to 6.697 Å), and somewhat more change along the two axes perpendicular to the chains (b axis: 5.142 Å to 5.112 Å ; c axis: 11.732 Å to 11.624 Å). With neutrons, we have determined the low-temperature $(T<4$ K) lattice constants to be $a=6.6870$ Å, and $b=5.0983$ Å. Throughout this paper we index wave-vector transfer in the corresponding reciprocal lattice: $\mathbf{Q}=h\mathbf{a}^*+k\mathbf{b}^*+l\mathbf{c}^*$, where $\mathbf{a}^*=(2\pi/a)\hat{\mathbf{a}}$, etc. We also define wave-vector transfer along the chain as $\tilde{q}\equiv\mathbf{Q}\cdot\mathbf{a}=2\pi h$.

The atomic coordinates and some of the important bond lengths and bond angles measured at $T=158$ K are listed in Tables I and II. Each copper ion is coordinated to two nitrogen atoms from the adjacent pyrazine rings (Cu-N1 = 1.973 Å) and two oxygen atoms (O1) from two different nitrate ions. The Cu-O1 distance equals 2.004 Å and is represented by a thick solid line in Fig. 2. The copper atoms and nitrate groups lie in mirror planes perpendicular to the twofold a axis. There is a semicoordinate bond between each copper

TABLE I. Fractional atomic coordinates and equivalent isotropic thermal parameters for CuPzN at $T=158$ K.

Atom	x	y	z	U
Cu1	0.0000	0.0000	0.0000	0.0071(3)
C1	0.3965(3)	-0.1709(5)	-0.0646(2)	0.0097(4)
N1	0.2947(5)	0.0000	0.0000	0.0086(7)
N2	0.0000	-0.2599(6)	0.1944(3)	0.0106(6)
O1	0.0000	-0.0116(4)	0.1723(3)	0.0104(6)
O2	0.0000	-0.4137(6)	0.1112(2)	0.0158(6)
O3	0.0000	-0.3310(6)	0.2952(2)	0.0208(6)
H1	0.319(5)	-0.291(6)	-0.105(3)	0.012

atom and a second oxygen (O2) from each nitrate group, represented by a thin line in Fig. 2. The Cu-O2 distance is 2.478 Å, which is much greater than the 1.9 Å for copper oxides with octahedral coordination, and the angle between the Cu-O2 bond and the normal to the Cu1-N1-O1 plane is 30.4°, which is also unfavorable for superexchange interactions. The O2 atoms also bridge the copper atoms to the copper sites on adjacent chains by a long pathway (3.264 Å, dashed lines). The axis connecting the Cu site to the $O2'$ site on the adjacent chain is tilted only 21.6° from the normal to the local coordination plane. This long interaction may help stabilize the formation of the three-dimensional lattice, but there is no evidence that it provides a superexchange pathway. The basal plane of the copper site is determined by the four short bonds. The strength of the superexchange interactions through the pyrazine rings will be a function of the angle between the normal to the basal plane and the normal to the (planar) pyrazine molecules; this angle is 51°.[27]

III. EXPERIMENTAL TECHNIQUES

Crystals of CuPzN were grown by slow evaporation of aqueous solutions of Cu(II) nitrate and the corresponding pyrazine (either protonated or deuterated). Large single crystals formed after several months. Faster evaporation results in the formation of many small, needle-shaped crystals.

Specific heat measurements on small, protonated crystals with typical mass $m=5$ mg were made in fields up to $\mu_0 H=9$ T for $0.1\ \mathrm{K}<T<10$ K using the relaxation method.[28,29] Magnetization measurements on both protonated and deuterated powder samples were carried out at the National High Field Magnet Laboratory in magnetic fields up to $\mu_0 H=30$ T using an EG&G vibrating sample magnetometer which had been calibrated against a high-purity nickel sample.

For inelastic neutron scattering, a sample was used that consisted of two deuterated crystals with total mass $m=72.8$ mg, coaligned to within 0.4° in the $(hk0)$ scattering plane. The measurements were performed on the SPINS cold neutron triple-axis spectrometer at NIST. For measurements requiring a nearly isotropic wave-vector resolution function we used a conventional parallel beam configuration. In this configuration the projection of the instrumental resolution ellipsoid on the scattering plane is an ellipse with principal directions approximately parallel and perpendicular to the wave-vector transfer **Q**, and a full width at half maximum (FWHM) along these directions of typically $\Delta Q_{\parallel}=0.02$ Å^{-1} and $\Delta Q_{\perp}=0.054$ Å^{-1}, respectively. For measurements requiring good **Q** resolution only along a single direction we used a horizontally focusing analyzer. With this configuration the principal axes of the projection of the resolution ellipsoid on the scattering plane are approximately parallel and perpendicular to the direction of the scattered beam $\hat{\mathbf{k}}_f$, and the FWHM were $\Delta Q_{\parallel}=0.045$ Å^{-1}, and $\Delta Q_{\perp}=0.32$ Å^{-1}, respectively. By orienting the spin chain axis parallel to $\hat{\mathbf{k}}_f$ the instrument effectively integrates over wave-vector transfer perpendicular to the chains. This led to a gain in intensity by a factor of 5.3 over the conventional parallel beam configuration without significant loss in wave-vector resolution along the chain axis. The projection of the resolution ellipsoid on the energy-transfer axis had FWHM $\Delta\hbar\omega=0.15$ meV in both configurations. The half-value contour of the projection of the resolution function of the focusing analyzer configuration onto the $\hbar\omega$-$\tilde{q}$ plane is shown in Fig. 1. We used 20 cm of beryllium oxide at $T=77$ K after the sample to reject neutrons with energies above the fixed final energy $E_f=3.7$ meV from the detection system, and 10 cm of beryllium at 50 K before the sample to suppress higher-order contamination of the incident beam for incident energies $E_i=E_f+\hbar\omega<5.1$ meV. The detector count rate was measured in units of the count rate of a monitor with sensitivity proportional to the incident wavelength. With this standard technique the raw count rates extracted from the experiment are proportional to the dynamic correlation function $\mathcal{S}(Q,\omega)$. For $E_i>5.1$ meV the beryllium filter prior to the sample was removed and corrections for higher-order contributions to the monitor count rate were applied so as once again to yield a measurement of $\mathcal{S}(Q,\omega)$.

TABLE II. Selected bond distances and angles for CuPzN at $T=158$ K.

Bond length	Bond angle
Cu1-N1 = 1.974(3) Å	N1-Cu1-O1=90°
Cu1-O1 = 2.004(3) Å	O1-Cu1-O2=56.88(9)°
Cu1-O2 = 2.478(3) Å	N1-Cu1-O2=90°

IV. EXPERIMENTAL RESULTS

A. Magnetization

The relative magnetization M/M_{sat} of a protonated powder sample of CuPzN at $T=4.2$ K and 1.8 K is shown in the main panel of Fig. 3 as a function of field up to $\mu_0 H=30$ T. Results from a deuterated sample at $T=4.2$ K were indistinguishable from the protonated sample. The data look similar to previous magnetization data for other one-dimensional spin-1/2 antiferromagnets.[30] The $T=1.82$ K data set has an initial slope 14% percent lower that of the 4.2-K set, but demonstrates an increasingly positive curvature, crossing the higher-temperature curve near 12 T and reaching saturation by 23 T. The data for both sets become measurably nonlinear with field for fields larger than 3 T. The trend of these data with decreasing temperature toward the indicated $T=0$ theoretical curve[31] is clearly apparent.

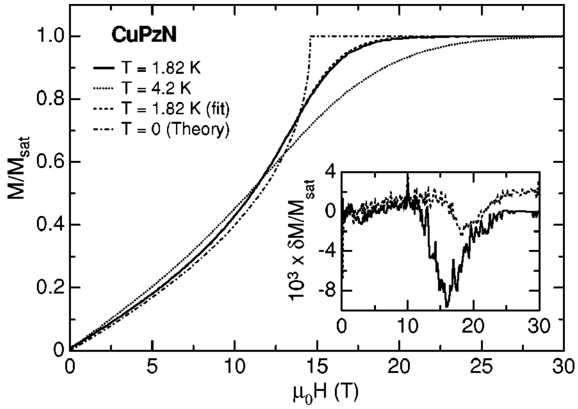

FIG. 3. Relative magnetization M/M_{sat} of CuPzN at $T=1.8$ K and 4.2 K. Dot-dashed line: calculated $T=0$ magnetization (Ref. 31) of an $S=1/2$ AFM chain with $J/k_B=10.3$ K. Dashed line: fit of $T=1.82$ K data to finite chain model described in text. The fit of the $T=4.2$ K curve is indistinguishable from the data. Inset: fit residuals $\delta M=M-M_{fit}$. Solid line: $T=1.8$ K; dashed line: $T=4.2$ K.

B. Specific heat

Figure 4 shows the temperature dependence of the total specific heat of CuPzN for a number of magnetic fields **H** parallel to **b**. As H is increased, the broad feature observed in zero field is suppressed, and the maximum gradually shifts to lower T. The solid lines are the results of a fit to a model based on exact diagonalization of short chains, as described below. The dashed line is the estimated phonon contribution determined from the fit.

Figure 5 shows an expanded view of the data in Fig. 4 for $T<1$ K, plotted as C/T vs T^2. In addition, the specific heat at $\mu_0H=9$ T parallel to **a** is shown. A predominantly linear in T behavior is observed. The positive slope visible at $\mu_0H=9$ T is a consequence of the field-induced shift of spectral weight to lower temperature. An increase in the linear part of $C(T)$ with increasing field is also seen. This indicates a renormalization of the spinon velocity with field, as will be discussed below.

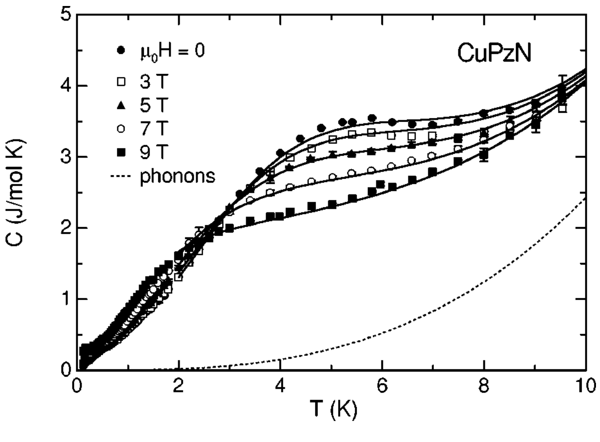

FIG. 4. Specific heat of CuPzN vs T at constant magnetic field $\mu_0H=0$, 3 T, 5 T, 7 T, and 9 T parallel to **b**. Solid lines are a fit to an exact diagonalization model as described in text. Dashed line is the phonon contribution determined from the fit.

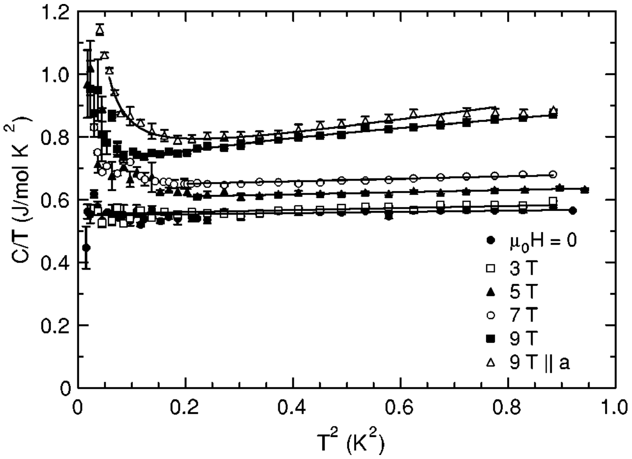

FIG. 5. Specific heat of CuPzN below $T=1$ K, plotted as C/T vs T^2 for at constant magnetic field $\mu_0H=0$, 3 T, 5 T, 7 T, and 9 T parallel to **b**, and $\mu_0H=9$ T parallel to **a**.

C. Neutron scattering

While bulk measurements have established that CuPzN is a quasi-one-dimensional magnet, such measurements cannot distinguish along which directions spins are coupled and along which directions they are not. For CuPzN both the **a** and **b** directions are candidate chain directions. To distinguish between these possibilities we measured the wave-vector dependence of the inelastic magnetic neutron-scattering cross section in the $(hk0)$ plane at low temperatures and for low values of energy transfer $\hbar\omega$. Figure 6(a) shows three scans along the $\mathbf{b}^*$ direction collected at $T=0.3$ K and $\hbar\omega=0.29$ meV, for three different values of wave-vector transfer along the perpendicular $\mathbf{a}^*$ axis (indicated as dots in Fig. 1). None of the scans shows any statistically significant modulation. There is, however, clearly more intensity for $\mathbf{Q}\cdot\mathbf{a}^*=\pi$ than for the other nearby values of this component of wave-vector transfer. This is brought out by Fig. 6(b), which shows the difference between the

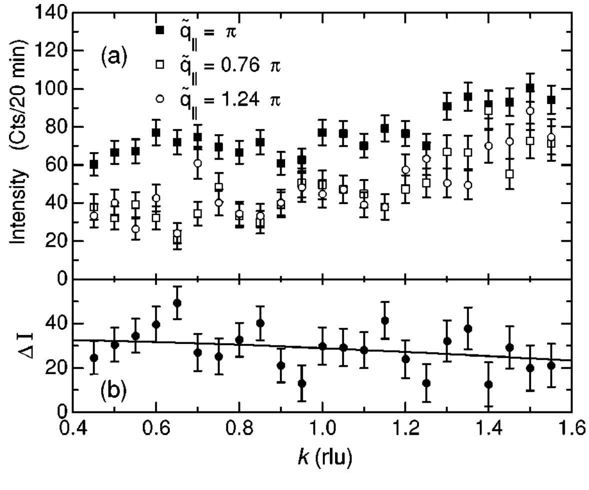

FIG. 6. Neutron-scattering intensity vs wave-vector transfer $k\mathbf{b}^*$ perpendicular to the chains at $\hbar\omega=0.29$ meV at $T=0.3$ K. (a) Raw data at $h=0.5$, 0.38, and 0.62 ($\tilde{q}=\pi,0.76\pi$, and 1.24π.) (b) Difference ΔI between $h=0.5$ scan and the average of the $h=0.38$ and $h=0.62$ scans. The lack of variation in ΔI with k shows the one dimensionality of the magnetic scattering in CuPzN.

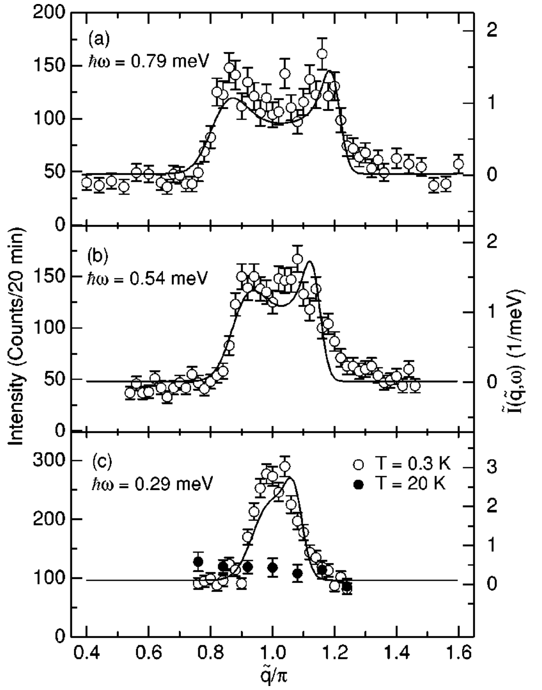

FIG. 7. Neutron-scattering intensity vs wave-vector transfer along the chains. Open symbols: $T=0.3$ K. Filled symbols: $T=20$ K. Right-hand axis gives normalized intensity scale as described in text. Solid lines are fit to a $T=0$ model for $\mathcal{S}(\tilde{q},\omega)$ (Ref. 11).

$\mathbf{Q}\cdot\mathbf{a}^{*}=\pi$ and the $\mathbf{Q}\cdot\mathbf{a}^{*}\neq\pi$ data. No modulation beyond that associated with the single-ion squared magnetic form factor (solid line) is observed, which indicates the absence of spin correlations along the $\mathbf{b}^{*}$ direction on a time scale $1/\omega=2$ ps for $k_BT\ll\hbar\omega$. This observation allows us to use the horizontally focusing analyzer to gain sensitivity by probing the $\mathbf{b}^{*}$-integrated intensity as we explore the $\tilde{q}\equiv\mathbf{Q}\cdot\mathbf{a}$ dependence of $\mathcal{S}(\mathbf{Q},\omega)$.

Data collected with the focusing analyzer are shown in Figs. 7 and 8. Figure 7 shows the inelastic scattering intensity versus wave-vector transfer $\tilde{q}$ along the chains at $T=0.3$ K for three fixed values of energy transfer $\hbar\omega=0.29$ meV, 0.54 meV, and 0.79 meV. Note that in all these scans wave-vector transfer along the $\mathbf{b}^{*}$ direction was varied so as to maintain $\mathbf{k_f}$ parallel to $\mathbf{a}^{*}$ as required to maintain good wave-vector resolution along the spin chain in the focusing analyzer configuration. At $\hbar\omega=0.29$ meV a single peak is observed at $\tilde{q}=\pi$, consistent with the data in Fig. 6. When the temperature is raised to $T=20$ K this peak disappears, as shown by the solid symbols in Fig. 7(c). This indicates that the inelastic scattering observed is indeed magnetic in origin. As $\hbar\omega$ is increased at $T=0.3$ K two peaks become visible, demonstrating the presence of dispersion along the chain direction. At $\hbar\omega=0.79$ meV, the two peaks are clearly resolved, but it is also apparent that the scattering cross section between the peaks is finite, which indicates a continuum contribution. The locations of the maxima in these constant-$\hbar\omega$ scans coincide with the lower bound of the spinon continuum anticipated for CuPzN on the basis of bulk measurements (see Fig. 1). Figure 8 shows the scattering intensity vs $\hbar\omega$ at $\tilde{q}=\pi/2$ (i.e., along the vertical line in Fig. 1). The abrupt increase in intensity at $\hbar\omega\approx1.3$ meV and the subsequent gradual decay at higher energies are again characteristic of the bounded spinon continuum. The solid lines in Figs. 7 and 8 were obtained from a fit to a model of the two-spinon contributions to $\mathcal{S}(\tilde{q},\omega)$ to be described below.

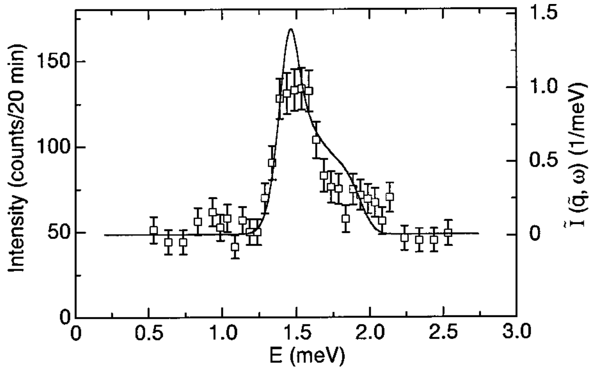

FIG. 8. Neutron-scattering intensity vs energy transfer at $\tilde{q}=\pi/2$ and $T=0.3$ K. Right-hand axis gives normalized intensity scale as described in text. The solid line is fit to a $T=0$ model for $\mathcal{S}(\tilde{q},\omega)$ (Ref. 11).

V. DISCUSSION

A. Magnetization

As is well known, many of the finite-temperature thermodynamic properties of quantum spin chains can be calculated quite accurately from exact diagonalization of short chains.[32] Comparison of data to calculations of this type is a very effective way of ascertaining how well a material is described by a particular model, and also of determining the exchange constants in that model. We now compare our results for the magnetization and specific heat of CuPzN to exact diagonalizations of linear chains containing up to $N=16$ spins 1/2.

For the magnetization, we find surprisingly good agreement between our data and the calculated result for $N=16$. We carried out a simultaneous fit to both data sets shown in Fig. 3 ($T=1.82$ and 4.2 K), using the measured average g factor $g_{avg}=2.11$. This fit gave $J/k_B=10.3(1)$ K.[33] The results of the fit are superimposed on the data in Fig. 3 but can only be distinguished from the data near $\mu_0H=15$ T at $T=1.82$ K. The residuals $\delta M=M-M_{fit}$ are shown in the inset of Fig. 3. These show the deviation of model from data to be significantly less than 1% over most of the field range. As a measure of the error in this fit associated with the finite system size used in the calculation, we have studied the convergence of $M(H,T,N)$ with increasing N. At $T=1.82$ K($k_BT/J=0.17$), the difference $[M(N=16)-M(N=15)]/M_{sat}$ is less than 0.003 for all H. At $T=4.2$ K, this difference is less than 2×10^{-5}. We conclude that our exact diagonalization results are representative of infinite length chains in the parameter range studied and that the magnetization of CuPzN down to $k_BT/J=0.17$ is perfectly described by the linear chain model.

B. Specific heat

At the high end of the temperature range accessed in our measurements, the specific heat may also be calculated accurately from exact diagonalization. Following Bonner and Fisher,[32] we compute the specific heat at constant field $C_H(J,T)$ as the average of that obtained from chains with 15 and 16 spins. Finite-size scaling suggests that this procedure gives quite accurate results down to temperatures $k_BT/J \approx 0.2$. All the data for $T>2$ K in Fig. 4 were fit simultaneously to

$$C(T)=AC_H(J,T)+BT^3, \tag{2}$$

where the second term accounts for the lattice contribution. As shown by the solid lines in Fig. 4, this model accounts for the data very well, with $A=1.05(1)$, $J/k_B=10.6(1)$ K, and $B=2.4(1)$ mJ/mol K^4. We ascribe the deviation of A from 1 to a systematic error in the normalization of our specific heat data. This is corroborated by a computation of the magnetic entropy from the specific heat data, which comes out to be 4% higher than the expected value of $R\ln 2$.[29]

The linear dispersion relation of the fermionic spinons at low energy implies that the low-temperature specific heat of the $S=1/2$ AFM chain should be linear in T. It is given by[34,35]

$$C_H(T)=\gamma_H T=\frac{\pi}{3}R\frac{k_BT}{v_s(H)}, \tag{3}$$

where $v_s(H)$ is the field-dependent spinon velocity. In zero field, $v_s=\pi J/2$, and the specific heat becomes $C=(2/3)Rk_BT/J$,[36,37] a result which has been confirmed experimentally in both copper benzoate[18] and CuPzN.[22] The field dependence of $v_s(H)$ can be determined from the Bethe ansatz[7,38] and used to predict $C_H(T)$. It is calculated as

$$v_s=\frac{E}{2\pi\sigma(\Lambda)}, \tag{4}$$

where E and σ are determined by the following set of integral equations:

$$\xi(\eta)=1-\frac{1}{2\pi}\int_{-\Lambda}^{\Lambda}K(\eta-\eta')\xi(\eta')d\eta',$$

$$\sigma(\eta)=\frac{1}{\pi(1+\eta^2)}-\frac{1}{2\pi}\int_{-\Lambda}^{\Lambda}K(\eta-\eta')\sigma(\eta')d\eta',$$

$$\rho(\eta)=\frac{1}{2\pi}\left[\frac{dK(\eta-\Lambda)}{d\eta}-\int_{-\Lambda}^{\Lambda}K(\eta-\eta')\rho(\eta')d\eta'\right],$$

$$E=\frac{4\Lambda}{(1+\Lambda^2)^2}+\int_{-\Lambda}^{\Lambda}\epsilon_0(\eta)\rho(\eta)d\eta, \tag{5}$$

with $K(\eta)=4/(4+\eta^2)$. The boundary of integration Λ is related to the magnetic field H by $g\mu_BH/J=2\pi\sigma(\Lambda)/\xi(\Lambda)$. In practice, we first fixed the value of Λ, and then solved the integral equations by numerical integration and iteration to obtain v_s and H. Accuracy of more than six digits can be achieved within minutes on a standard workstation. We performed the calculation for many values of Λ to give v_s as a smooth function of H, which is shown in the inset to Fig. 9. This determines the theoretical curve of the coefficient $\gamma(H)$ with no adjustable parameters, once J and the g value are fixed.

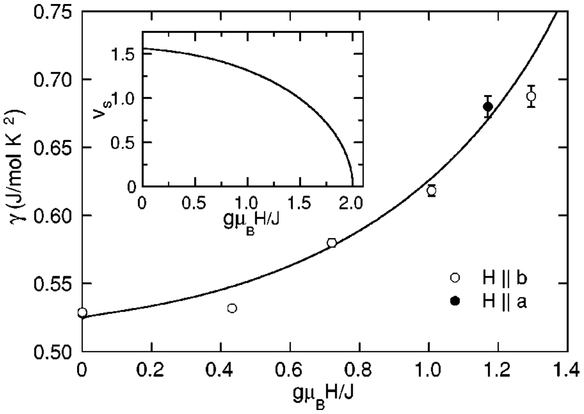

FIG. 9. Field dependence of the Sommerfeld constant ($\gamma=\lim_{T\to 0}C/T$) derived from low-T specific-heat data, compared to Bethe-ansatz calculation (solid line). The data were scaled by a factor 0.95 to account for a systematic error in normalization that was derived from the comparison to exact diagonalization data shown in Fig. 4. Inset: calculated field dependence of the spinon velocity $v_s(H)$.

Figure 9 shows the measured field dependence of $\gamma_H=C_H/T$ determined from the data in Fig. 5, together with the calculated result. These are plotted against reduced field $H^*=g\mu_BH/J$ with $J/k_B=10.6$ K, and $g_a=2.05$ and $g_b=2.27$.[25] Note that for this comparison a correction factor $1/A=0.95$ was applied to the specific-heat data to account for the normalization error discovered when comparing to exact diagonalization calculations. The agreement between model and data is excellent and the data provides direct experimental evidence for the field dependence of the spinon velocity in the $S=1/2$ AFM chain.

C. Neutron scattering

The magnetic contribution to the measured inelastic neutron-scattering signal is proportional to the normalized magnetic scattering intensity

$$\tilde{I}(\mathbf{Q},\omega)=\left|\frac{g}{2}F(Q)\right|^2\sum_{\alpha\beta}(\delta_{\alpha\beta}-\hat{\mathbf{Q}}_{\boldsymbol{\alpha}}\hat{\mathbf{Q}}_{\boldsymbol{\beta}})\tilde{\mathcal{S}}^{\alpha\beta}(\mathbf{Q},\omega). \tag{6}$$

In this expression $F(Q)$ is the magnetic form factor of Cu^{2+},[39] and $\tilde{\mathcal{S}}^{\alpha\beta}(\mathbf{Q},\omega)$ is the convolution of the dynamic spin-correlation function,[40]

$$\mathcal{S}^{\alpha\beta}(\mathbf{Q},\omega)=\frac{1}{2\pi\hbar}\int dte^{i\omega t}\frac{1}{N}\times\sum_{\mathbf{RR}'}\langle S_{\mathbf{R}}^{\alpha}(t)S_{\mathbf{R}'}^{\beta}(0)\rangle e^{-i\mathbf{Q}\cdot(\mathbf{R}-\mathbf{R}')}, \tag{7}$$

with the normalized instrumental resolution function.[41] We determined $\tilde{I}(\mathbf{Q},\omega)$ in absolute units by comparison of the magnetic scattering intensity to the incoherent scattering intensity I_V from a vanadium reference sample:

$$\tilde{I}(\mathbf{Q},\omega)=\left[\frac{1}{\int I_V d\hbar\omega}\,\frac{n_V}{n_{Cu}}\left(\frac{b_i}{r_0}\right)^2\right]I_{mag}(\mathbf{Q},\omega). \tag{8}$$

Here n_V and n_{Cu} are the number of moles of vanadium and copper in the reference and sample, respectively, $b_i=6.36$ fm is the incoherent scattering length for vanadium,[40] $r_0=5.38$ fm, and $I_{mag}(\mathbf{Q},\omega)$ is the portion of the measured signal attributable to magnetic scattering. The conversion of the measured count rates to $\tilde{I}(\mathbf{Q},\omega)$ is shown on the right-hand axis in Figs. 7 and 8. As a complete, independent measure of the nonmagnetic background was not made, the zero of the $\tilde{I}(\mathbf{Q},\omega)$ scale was set from the backgrounds determined in fitting the data.

Müller *et al.*[11] proposed the following approximate expression for the $T=0$ dynamic spin-correlation function for the spin-1/2 Heisenberg AFM chain:

$$\mathcal{S}^{\alpha\alpha}(\tilde{q},\omega)=\frac{1}{2\pi}\,\frac{\tilde{A}}{\sqrt{(\hbar\omega)^2-\epsilon_1^2(\tilde{q})}}\,\Theta(\hbar\omega-\epsilon_1(\tilde{q}))\times\Theta(\epsilon_2(\tilde{q})-\hbar\omega). \tag{9}$$

In this expression $\Theta(x)$ is the step function, while $\epsilon_1(\tilde{q})=(\pi J/2)|\sin\tilde{q}|$ and $\epsilon_2(\tilde{q})=\pi J\sin\tilde{q}/2$ are the lower and upper bounds of the spinon continuum. Recent publications present exact calculations of the contribution to $\mathcal{S}(\tilde{q},\omega)$ from n-spinon excitations.[10,42,43] The numerical differences between the exact expressions for $\mathcal{S}(\tilde{q},\omega)$ and the simpler approximate form are small, and are unimportant for the analysis of our relatively low statistics scattering data for CuPzN. For the purpose of determining whether the scattering data can be described by the spin chain model that accounted for our bulk data we have therefore used Eq. (9). This expression was convolved with the experimental resolution function and the overall scale factor $\tilde{A}$, the exchange constant J, and a constant background for each scan were varied to achieve the best possible fit to the scattering data. The results of this fit with $\tilde{A}=3.5(1)$ and $J=0.90(1)$ meV are shown as solid lines in Figs. 7 and 8, and may be seen to provide an excellent description of the data. The value of J derived from neutron scattering is indistinguishable from that derived from specific heat data.

VI. CONCLUSION

The combination of magnetization, specific heat, and inelastic neutron scattering reported here show that CuPzN is extremely well described by the simple isotropic Heisenberg model of the $S=1/2$ AFM spin chain with $J=0.90(1)$ meV. The neutron-scattering measurements have confirmed that the crystalline **a** axis is the one-dimensional chain axis, as had been predicted from structural analysis. The field dependence of the specific heat shows that CuPzN remains gapless in a field and that the spinon velocity is reduced in agreement with predictions based on calculations using the Bethe-ansatz technique. Taken as a whole, these results establish that CuPzN is an excellent model system for the one-dimensional spin-1/2 Heisenberg antiferromagnet even in large magnetic fields ($g\mu_B H/J\lesssim 1.4$) and at low temperatures ($k_B T/J\gtrsim 0.03$). This material is therefore an excellent candidate for further studies of the unique field-dependent quantum critical properties of the spin-1/2 Heisenberg antiferromagnet.

ACKNOWLEDGMENTS

NSF Grants No. DMR-9357518 and No. DMR-9453362 supported work at JHU. This work utilized neutron research facilities supported by NIST and the NSF under Agreement No. DMR-9423101. A portion of this work was performed at the National High Magnetic Field Laboratory, which is supported by NSF cooperative agreement No. DMR-9527035 and the State of Florida. D.H.R. acknowledges support from the David and Lucile Packard Foundation.

---

[1] S. Chakravarty, B. I. Halperin, and D. R. Nelson, Phys. Rev. B **39**, 2344 (1989).

[2] S. Sachdev, in *Dynamical Properties of Unconventional Magnetic Systems*, Vol. 349 of *NATO Advanced Study Institute, Series E: Applied Sciences*, edited by A. T. Skjeltorp and D. Sherrington (Kluwer Academic, Dordrecht, 1998).

[3] G. Aeppli and C. Broholm, in *Handbook on the Physics and Chemistry of Rare Earths*, edited by K. A. Gschneidner, Jr., L. Eyring, G. H. Lander, and G. R. Choppin (Elsevier, Amsterdam, 1994), Vol. 19, Chap. 131, p. 123.

[4] V. J. Emery and S. A. Kivelson, Physica C **263**, 44 (1996).

[5] C. Castellani, C. Di Castro, and M. Grilli, J. Supercond. **9**, 413 (1996).

[6] S. R. Julian, F. V. Carter, F. M. Grosche, R. K. W. Haselwimmer, S. J. Lister, N. D. Mathur, G. J. McMullan, C. Pfleiderer, S. S. Saxena, I. R. Walker, N. J. W. Wilson, and G. G. Lonzarich, J. Magn. Magn. Mater. **177-181**, 265 (1998).

[7] N. M. Bogoliubov, A. G. Izergin, and V. E. Korepin, Nucl. Phys. B **275**, 687 (1986).

[8] A. Fledderjohann, C. Gerhardt, K. H. Mütter, A. Schmitt, and M. Karbach, Phys. Rev. B **54**, 7168 (1997).

[9] J. F. Audet, A. Fledderjohann, C. Gerhardt, M. Karbach, H. Kroeger, K. H. Mütter, and M. Schmidt, in *Theory of Spin Lattices and Lattice Gauge Models,* Proceedings of the 165th WE-Heraeus-Seminar, edited by J. W. Clark and M. L. Ristig (Springer-Verlag, Berlin, 1997), p. 41.

[10] M. Karbach, G. Muller, A. H. Bougourzi, A. Fledderjohann, and K. H. Mütter, Phys. Rev. B **55**, 12 510 (1997).

[11] G. Müller, H. Thomas, H. Beck, and J. C. Bonner, Phys. Rev. B **24**, 1429 (1981).

[12] L. Fadeev, in *Recent Advances in Field Theory and Statistical Physics,* Proceedings of the Les Houches Summer School of Theoretical Physics, Les Houches, 1982, Session XXXIX, edited by L. B. Zuber and R. Stora (North-Holland, Amsterdam, 1984); J. Lowenstein, *ibid.*

[13] A. M. Tsvelik, *Quantum Field Theory in Condensed Matter Physics* (Cambridge University Press, Cambridge, 1995).

[14] I. U. Heilmann, G. Shirane, Y. Endoh, R. J. Birgeneau, and S. L.

Holt, Phys. Rev. B **18**, 3530 (1978).

[15] D. A. Tennant, T. G. Perring, R. A. Cowley, and S. E. Nagler, Phys. Rev. Lett. **70**, 4003 (1993).

[16] R. Coldea, D. A. Tennant, R. A. Cowley, D. F. McMorrow, B. Dorner, and Z. Tylczynski, Phys. Rev. Lett. **79**, 151 (1997).

[17] D. C. Dender, D. Davidović, D. H. Reich, C. Broholm, K. Lefmann, and G. Aeppli, Phys. Rev. B **53**, 2583 (1996).

[18] D. C. Dender, P. R. Hammar, D. H. Reich, C. Broholm, and G. Aeppli, Phys. Rev. Lett. **79**, 1750 (1997).

[19] M. Oshikawa and I. Affleck, Phys. Rev. Lett. **79**, 2883 (1997).

[20] F. H. L. Essler and A. M. Tsvelik, Phys. Rev. B **57**, 10 592 (1998).

[21] D. B. Losee, H. W. Richardson, and W. E. Hatfield, J. Chem. Phys. **59**, 3600 (1973).

[22] G. Mennenga, L. J. de Jongh, W. J. Huiskamp, and J. Reedijk, J. Magn. Magn. Mater. **44**, 89 (1984).

[23] J. Villain and J. M. Loveluck, J. Phys. (France) Lett. **38**, L77 (1977).

[24] A. Santoro, A. D. Mighell, and C. W. Reimann, Acta Crystallogr., Sect. B: Struct. Crystallogr. Cryst. Chem. **26**, 9979 (1970).

[25] K. T. McGregor and S. G. Soos, J. Chem. Phys. **64**, 2506 (1976).

[26] Structural determination parameters: $a=6.697(1)$ Å, $b=5.112(1)$ Å, $c=11.624(3)$ Å at $T=158$ K, Z = 2, space group $Pmna$. A total of 888 reflections were observed, of which 619 were unique. $R=0.0508$ based on the 541 reflections with $I>4\sigma(I)$. $R=0.0564$ based on all unique reflections.

[27] H. W. Richardson and W. E. Hatfield, J. Am. Chem. Soc. **98**, 835 (1976).

[28] R. Bachmann, F. J. DiSalvo, T. H. Geballe, R. L. Greene, R. E. Howard, C. N. King, H. C. Kirsch, K. N. Lee, R. E. Schwall, H-U. Thomas, and R. B. Zubeck, Rev. Sci. Instrum. **43**, 205 (1972).

[29] P. R. Hammar, Ph.D. thesis, Johns Hopkins University, 1998.

[30] H. Mollymoto, E. Fujiwara, M. Motokawa, and M. Date, J. Phys. Soc. Jpn. **48**, 1771 (1980).

[31] R. B. Griffiths, Phys. Rev. A **133**, A768 (1964).

[32] J. C. Bonner and M. E. Fisher, Phys. Rev. **135**, A640 (1964).

[33] This was actually a three-parameter fit. In addition to J it was necessary to include offsets to account for small, field-independent backgrounds arising from offset voltages in the measuring electronics. These backgrounds are $0.007M_{sat}$ and $0.006M_{sat}$ for the $T=1.82$ and 4.2 K data, respectively.

[34] H. W. J. Blöte, J. L. Cardy, and M. P. Nightingale, Phys. Rev. Lett. **56**, 742 (1986).

[35] I. Affleck, Phys. Rev. Lett. **56**, 746 (1986).

[36] M. Takahashi, Prog. Theor. Phys. **50**, 1519 (1973).

[37] J. D. Johnson and B. M. McCoy, Phys. Rev. A **6**, 1613 (1972).

[38] V. E. Korepin, N. M. Bogoliubov, and A. G. Izergin, *Quantum Inverse Scattering Method and Correlation Functions* (Cambridge University Press, Cambridge, 1993), and references therein.

[39] A. J. Freeman and R. E. Watson, Acta Crystallogr. **14**, 231 (1961).

[40] We use the notation of S. W. Lovesey, *Theory of Neutron Scattering from Condensed Matter* (Clarendon Press, Oxford, 1984).

[41] N. D. Chesser and J. D. Axe, Acta Crystallogr., Sect. A: Cryst. Phys., Diffr., Theor. Gen. Crystallogr. **29**, 160 (1973).

[42] A. H. Bougourzi, M. Couture, and M. Kacir, Phys. Rev. B **54**, R12 669 (1997).

[43] A. Abada, A. H. Bougourzi, and B. Si-Lakhal, Nucl. Phys. B **497**, 733 (1997).